

---

# Set2Graph: Learning Graphs From Sets

---

Hadar Serviansky<sup>1</sup> Nimrod Segol<sup>1</sup> Jonathan Shlomi<sup>1</sup>  
Kyle Cranmer<sup>2</sup> Eilam Gross<sup>1</sup> Haggai Maron<sup>3</sup> Yaron Lipman<sup>1</sup>

## Abstract

Many problems in machine learning (ML) can be cast as learning functions from sets to graphs, or more generally to hypergraphs; in short, Set2Graph functions. Examples include clustering, learning vertex and edge features on graphs, and learning triplet data in a collection.

Current neural network models that approximate Set2Graph functions come from two main ML sub-fields: equivariant learning, and similarity learning. Equivariant models would be in general computationally challenging or even infeasible, while similarity learning models can be shown to have limited expressive power.

In this paper we suggest a neural network model family for learning Set2Graph functions that is both practical and of maximal expressive power (universal), that is, can approximate arbitrary continuous Set2Graph functions over compact sets. Testing our models on different machine learning tasks, including an application to particle physics, we find them favorable to existing baselines.

## 1. Introduction

We consider the problem of learning functions mapping sets of vectors in  $\mathbb{R}^{d_{in}}$  to graphs, or more generally hypergraphs; we name this problem Set2Graph, or set-to-graph. Set-to-graph functions appear in machine-learning applications such as clustering, predicting features on edges and nodes in graphs, and learning  $k$ -edge information in sets.

Mathematically, we represent each set-to-graph function as a collection of set-to- $k$ -edge functions, where each set-to- $k$ -edge function learns features on  $k$ -edges. That is, given an input set  $\mathcal{X} = \{\mathbf{x}_1, \dots, \mathbf{x}_n\} \subset \mathbb{R}^{d_{in}}$  we consider functions  $\mathbf{F}^k$  attaching feature vectors to  $k$ -edges: each  $k$ -tuple  $(\mathbf{x}_{i_1}, \dots, \mathbf{x}_{i_k})$  is assigned with an output vector  $\mathbf{F}^k(\mathcal{X})_{i_1, i_2, \dots, i_k} \in \mathbb{R}^{d_{out}}$ . Now, functions mapping sets to hypergraphs with hyper-edges of size up-to  $k$  are modeled

<sup>1</sup>Weizmann Institute of Science, Rehovot, Israel <sup>2</sup>New York University, New-York, USA <sup>3</sup>NVIDIA Research.

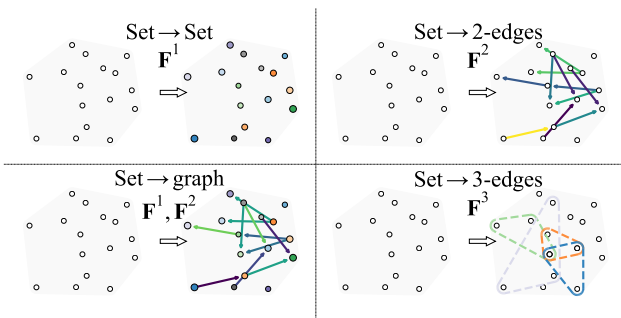


Figure 1. Set-to-graph functions are represented as collections of set-to- $k$ -edge functions.

by  $(\mathbf{F}^1, \mathbf{F}^2, \dots, \mathbf{F}^k)$ . For example, functions mapping sets to standard graphs are represented by  $(\mathbf{F}^1, \mathbf{F}^2)$ , see Figure 1.

Set-to-graph functions are well-defined if they satisfy a property called *equivariance* (defined later), and therefore the set-to-graph problem is an instance of the bigger class of equivariant learning. One option to learn equivariant set-to-graph model is using out-of-the-box full equivariant model as in (Maron et al., 2019b). By full we mean that each linear layer is chosen from the space of *all* linear equivariant layers. Learning  $\mathbf{F}^k$  would require equivariant layers mapping 1-st order tensors (representing sets) to  $k$ -order tensors (representing  $k$ -edge hypergraphs). Such models will be infeasible computationally: (i) They will possess a large number of parameters (combinatorial in  $k$ ); (ii) they will require storing in memory  $k$ -th order tensors.

Aside from the practical problem of using equivariant models for learning set-to-graph functions, there is a theoretical question of expressive power, or *universality*. That is, the ability of the models to approximate any continuous equivariant function. In equivariant learning literature set-to-set models (Zaheer et al., 2017; Qi et al., 2017) are recently proven equivariant universal (Keriven & Peyré, 2019; Segol & Lipman, 2020; Sannai et al., 2019). In contrast, the situation for graph-to-graph equivariant models is more intricate: some models, such as message passing (a.k.a. graph convolutional networks), are known to be non-universal (Xu et al., 2019; Morris et al., 2018; Maron et al., 2019a; Chen et al., 2019); high-order equivariant models are known to be universal (Maron et al., 2019c) but as discussed above, not

practical. Universality of equivariant set-to-graph models is not known, as far as we are aware.

Another machine-learning approach for learning set-to-graph functions is similarity learning (Bromley et al., 1994; Chopra et al., 2005; Simo-Serra et al., 2015; Zagoruyko & Komodakis, 2015; Bell & Bala, 2015; Ahmed et al., 2015; Vo & Hays, 2016) This is a simpler approach where a siamese network  $\phi$  is used to embed each set element independently  $\mathbf{y}_i = \phi(\mathbf{x}_i)$  and pairwise information is extracted from pairs of embeddings  $\psi(\mathbf{y}_i, \mathbf{y}_j)$ . Although this approach does not suffer from the complexity issues of equivariant network it has limited expressive power.

In this paper we introduce a model for the set-to-graph problem that is both *practical* (i.e., small number of parameters and no-need to build high-order tensors in memory) and *provably universal*. We achieve that with models defined as composition of three networks:  $\mathbf{F}^k = \psi \circ \beta \circ \phi$ , where  $\phi$  is a set-to-set model,  $\beta$  is a *non-learnable* broadcasting set-to-graph layer, and  $\psi$  is a simple graph-to-graph network using only a single Multi-Layer Perceptron (MLP) acting on each  $k$ -edge feature vector independently.

We have tested our model on four different applications: (i) *Set-to-2-edges*: partitioning (clustering) of simulated particles generated in the Large Hadron Collider (LHC); (ii) *Set-to-2-edges*: predicting Delaunay edges in planar point clouds; (iii) *Set-to-graph*: improving graph neural networks by augmenting them with a set-2-graph models; and (iv) *Set-to-3-edges*: finding triplets of point on the convex hull of a volumetric point cloud. We show that in all applications we achieve superior performances to baseline.

## 2. Previous work

**Equivariant learning.** In many learning setups the task we would like to learn is invariant or equivariant to certain transformations of the input. The Canonical examples are image classification tasks (LeCun et al., 1998; Krizhevsky et al., 2012) which are often assumed to be invariant to translations of the image, and set classification tasks (Zaheer et al., 2017; Qi et al., 2017) which are typically invariant to the specific order of the elements in the set. Restricting models to be invariant or equivariant to these transformation was shown to be an excellent approach for reducing the number of parameters of models while improving generalization. This paradigm for designing deep models was used for many different tasks, data modalities and transformations, e.g., set learning (Zaheer et al., 2017; Qi et al., 2017), graph learning (Kipf & Welling, 2016; Gilmer et al., 2017; Veličković et al., 2017; Xu et al., 2019; Kondor et al., 2018; Maron et al., 2019b;a), learning images with rotational and reflectional symmetries (Cohen & Welling, 2016a;b; Dieleman et al., 2016; Worrall et al., 2017), learning functions on spheres

(Cohen et al., 2018; Esteves et al., 2017) and learning general 3D data (Weiler et al., 2018; Worrall & Brostow, 2018; Weiler et al., 2018). Except from designing invariant and equivariant networks there has been a keen interest in the analysis of such models (Ravanbakhsh et al., 2017; Kondor et al., 2018), especially the analysis of their approximation power (Zaheer et al., 2017; Qi et al., 2017; Maron et al., 2019c; Keriven & Peyré, 2019; Segol & Lipman, 2020). Most related to this work is, the work of (Maron et al., 2019b) which characterized equivariant layers between hypergraph data which includes the set-to-graph setup, (Maron et al., 2019c) that proved a universal approximation property for invariant networks for general permutation groups, and the work of (Keriven & Peyré, 2019) which provides a proof that equivariant neural networks  $\mathbb{R}^n \rightarrow \mathbb{R}^{n^k}$  are universal. They construct an equivariant network with a single hidden layer that may contain tensors of unbounded degree. In contrast we construct equivariant networks  $\mathbb{R}^n \rightarrow \mathbb{R}^{n^k}$  that only involve tensors of order 1 and  $k$  and are universal.

**Learning to Cluster.** Deep clustering is a large field (Aljalbout et al., 2018) and we restrict our attention to the methods that are most related to ours. The work that tackles the most similar problem to this paper is the work of (Jiang & Verma, 2019) that suggest a method for meta clustering that is based on LSTMs and therefore depends on the order of the set elements. In contrast, our method is blind (equivariant) to the chosen order of the input sets. In another related work, (Hsu et al., 2017) suggest to perform transfer learning between tasks and domains by learning how to cluster, where the main idea is to learn a similarity function between set elements according to their labels. This similarity function is learned using a loss that promotes cluster assignments of points with the same label. The main difference from our work is the fact that we assume that all the data can be seen at the same time and aim at universal models approximating set-to-graph functions.

We discuss the differences of our method and equivariant, similarity learning (including learning to cluster) methods in more details at the end of Section 4.

## 3. Learning hypergraphs from sets

We would like to learn functions mapping sets of  $n$  vectors in  $\mathbb{R}^{d_{in}}$  to hypergraphs with  $n$  nodes (think of the nodes as corresponding to the set elements), and arbitrary  $k$ -edge feature vectors in  $\mathbb{R}^{d_{out}}$ , where a  $k$ -edge is defined as a  $k$ -tuple of set elements. A function mapping sets of vectors to  $k$ -edges is called set-to- $k$ -edge function and denoted  $\mathbf{F}^k : \mathbb{R}^{n \times d_{in}} \rightarrow \mathbb{R}^{n^k \times d_{out}}$ . Consequently, a set-to-hypergraph function would be modeled as a sequence  $(\mathbf{F}^1, \mathbf{F}^2, \dots, \mathbf{F}^K)$ , for target hypergraphs with hyperedges of maximal size  $K$ . For example,  $\mathbf{F}^2$  learns pairwise relations in a set; and  $(\mathbf{F}^1, \mathbf{F}^2)$  is a function from sets to graphs; see Figure 1.

**Our goal** is to design equivariant neural network models for  $\mathbf{F}^k$  that are as-efficient-as-possible in terms of number of parameters and memory usage, but on the same time with maximal expressive power, i.e., universal.

**Representing sets and  $k$ -edges.** A matrix  $\mathbf{X} = (\mathbf{x}_1, \mathbf{x}_2, \dots, \mathbf{x}_n)^T \in \mathbb{R}^{n \times d_{\text{in}}}$  represents a set of  $n$  vectors  $\mathbf{x}_i \in \mathbb{R}^{d_{\text{in}}}$  and therefore should be considered up to re-ordering of its rows. We denote by  $S_n = \{\sigma\}$  the symmetric group, that is the group of bijections (permutations)  $\sigma : [n] \rightarrow [n]$ , where  $[n] = \{1, \dots, n\}$ . We denote by  $\sigma \cdot \mathbf{X}$  the matrix resulting in reordering the rows of  $\mathbf{X}$  by the permutation  $\sigma$ , i.e.,  $(\sigma \cdot \mathbf{X})_{i,j} = \mathbf{X}_{\sigma^{-1}(i),j}$ . In this notation,  $\mathbf{X}$  and  $\sigma \cdot \mathbf{X}$  represent the same set, for all permutations  $\sigma$ .

$k$ -edges are represented as a tensor  $\mathbf{Y} \in \mathbb{R}^{n^k \times d_{\text{out}}}$ , where  $\mathbf{Y}_{i,:} \in \mathbb{R}^{d_{\text{out}}}$  denotes the feature vector attached to the  $k$ -edge defined by the  $k$ -tuple  $(\mathbf{x}_{i_1}, \mathbf{x}_{i_2}, \dots, \mathbf{x}_{i_k})$ , where  $\mathbf{i} = (i_1, i_2, \dots, i_k) \in [n]^k$  is a multi-index with non-repeating indices. Similarly to the set case,  $k$ -edges are considered up to renumbering of the nodes by some permutation  $\sigma \in S_n$ . That is, if we define the action  $\sigma \cdot \mathbf{Y}$  by  $(\sigma \cdot \mathbf{Y})_{\mathbf{i},j} = \mathbf{Y}_{\sigma^{-1}(\mathbf{i}),j}$ , where  $\sigma^{-1}(\mathbf{i}) = (\sigma^{-1}(i_1), \sigma^{-1}(i_2), \dots, \sigma^{-1}(i_k))$ , then  $\mathbf{Y}$  and  $\sigma \cdot \mathbf{Y}$  represent the same  $k$ -edge data, for all  $\sigma \in S_n$ .

**Equivariance.** For  $\mathbf{F}^k$  to represent a well-defined map between sets  $\mathbf{X} \in \mathbb{R}^{n \times d_{\text{in}}}$  and  $k$ -edge data  $\mathbf{Y} \in \mathbb{R}^{n^k \times d_{\text{out}}}$  it should be *equivariant* to permutations, namely satisfy

$$\mathbf{F}^k(\sigma \cdot \mathbf{X}) = \sigma \cdot \mathbf{F}^k(\mathbf{X}), \quad (1)$$

for all sets  $\mathbf{X} \in \mathbb{R}^{n \times d_{\text{in}}}$  and permutations  $\sigma \in S_n$ . Equivariance guarantees, in particular, that the two equivalent sets  $\mathbf{X}$  and  $\sigma \cdot \mathbf{X}$  are mapped to equivalent  $k$ -edge data tensors  $\mathbf{F}^k(\mathbf{X})$  and  $\sigma \cdot \mathbf{F}^k(\mathbf{X})$ .

**Set-to- $k$ -edge models.** In this paper we explore the following neural network model family for approximating  $\mathbf{F}^k$ :

$$\mathbf{F}^k(\mathbf{X}; \theta) = \psi \circ \beta \circ \phi(\mathbf{X}), \quad (2)$$

where  $\phi, \beta$ , and  $\psi$  will be defined soon. For  $\mathbf{F}^k$  to be equivariant (as required in equation 1) it is sufficient to require its constituents, namely  $\phi, \beta, \psi$ , are equivariant. That is,  $\phi, \beta, \psi$  all satisfy equation 1.

**Set-to-graphs models.** Given the model of set-to- $k$ -edge functions, a model for a set-to-graph function can now be constructed from a pair of set-to- $k$ -edge networks  $(\mathbf{F}^1, \mathbf{F}^2)$ . Similarly, set-to-hypergraph function would require  $(\mathbf{F}^1, \dots, \mathbf{F}^K)$ , where  $K$  is the maximal hyperedge size. Figure 1 shows an illustration of set-to- $k$ -edge and set-to-graph functions

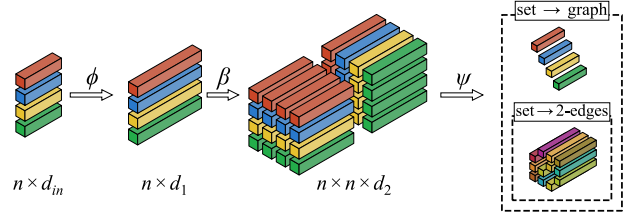


Figure 2. The model architecture for the Set-to-graph and set-to-2-edge functions.

**$\phi$  component.**  $\phi : \mathbb{R}^{n \times d_{\text{in}}} \rightarrow \mathbb{R}^{n \times d_1}$  is a set-to-set equivariant model, that is  $\phi$  is mapping sets of vectors in  $\mathbb{R}^{d_{\text{in}}}$  to sets of vectors in  $\mathbb{R}^{d_1}$ . To achieve the universality goal we will need  $\phi$  to be universal as set-to-set model; that is,  $\phi$  can approximate arbitrary continuous set-to-set functions. Several options exist (Keriven & Peyré, 2019; Sannai et al., 2019) although probably the simplest option is either DeepSets (Zaheer et al., 2017) or one of its variations; all were proven to be universal recently in (Segol & Lipman, 2020).

In practice, as will be clear later from the proof of the universality of the model, when building set-to-graph or set-to-hypergraph model, the  $\phi$  (set-to-set) part of the  $k$ -edge networks can be shared between different set-to- $k$ -edge models,  $\mathbf{F}^k$ , without compromising universality.

**$\beta$  component.**  $\beta : \mathbb{R}^{n \times d_1} \rightarrow \mathbb{R}^{n^k \times d_2}$  is a non-learnable linear *broadcasting layer* mapping sets to  $k$ -edges. In theory, as shown in (Maron et al., 2019b) the space of equivariant linear mappings  $\mathbb{R}^{n \times d_1} \rightarrow \mathbb{R}^{n^k \times d_2}$  is of dimension  $d_1 d_2 \text{bell}(k+1)$  which can be very high since bell has exponential growth. Interestingly, in the set-to- $k$ -edge case one can achieve universality with only  $k$  linear operators. We define the broadcasting operator to be

$$\beta(\mathbf{X})_{\mathbf{i},:} = [\mathbf{x}_{i_1}, \mathbf{x}_{i_2}, \dots, \mathbf{x}_{i_k}], \quad (3)$$

where  $\mathbf{i} = (i_1, \dots, i_k)$  and brackets denote concatenation in the feature dimension, that is, for  $\mathbf{A} \in \mathbb{R}^{n^k \times d_a}$ ,  $\mathbf{B} \in \mathbb{R}^{n^k \times d_b}$  their concatenation is  $[\mathbf{A}, \mathbf{B}] \in \mathbb{R}^{n^k \times (d_a + d_b)}$ . Therefore, the feature output dimension of  $\beta$  is  $d_2 = k d_1$ .

As an example, consider the graph case, where  $k = 2$ . In this case  $\beta(\mathbf{X})_{i_1, i_2} = [\mathbf{x}_{i_1}, \mathbf{x}_{i_2}]$ . This function is illustrated in Figure 2 broadcasting data in  $\mathbb{R}^{n \times d_1}$  to tensor  $\mathbb{R}^{n \times n \times d_2}$ .

To see that broadcasting layer is equivariant, it is enough to consider a single feature  $\beta(\mathbf{X})_{\mathbf{i}} = \mathbf{x}_{i_1}$ . Permuting the rows of  $\mathbf{X}$  by a permutation  $\sigma$  we get  $\beta(\sigma \cdot \mathbf{X})_{\mathbf{i},j} = \mathbf{x}_{\sigma^{-1}(i_1),j} = \beta(\mathbf{X})_{\sigma^{-1}(\mathbf{i}),j} = (\sigma \cdot \beta(\mathbf{X}))_{\mathbf{i},j}$ .

**$\psi$  component.**  $\psi : \mathbb{R}^{n^k \times d_2} \rightarrow \mathbb{R}^{n^k \times d_{\text{out}}}$  is a mapping of  $k$ -tensors to  $k$ -tensors. Here the theory of equivariant operators indicates that the space of linear equivariant maps

is of dimension  $d_2 d_{\text{out}} \text{bell}(2k)$  that suggests a huge number of model parameters even for a single linear layer. Surprisingly, universality can be achieved with much less, in fact a single linear operator (i.e., scaled identity) in each layer which in the multi-feature multi-layer case boils to applying a Multi-Layer Perceptron  $\mathbf{m} : \mathbb{R}^{d_2} \rightarrow \mathbb{R}^{d_{\text{out}}}$  to each feature in the input tensor  $\mathbf{X} \in \mathbb{R}^{n^k \times d_2}$ . That is, we use

$$\psi(\mathbf{X})_{i,:} = \mathbf{m}(\mathbf{X}_{i,:}). \quad (4)$$

Figure 2 illustrates set-to-2-edges and set-to-graph models incorporating the three components  $\phi, \beta, \psi$  discussed above.

#### 4. Universality of set-to-graph models.

In this section we prove that the model  $\mathbf{F}^k$  introduced above, is universal, in the sense it can approximate arbitrary continuous equivariant set-to- $k$ -edge functions  $\mathbf{G}^k : \mathbb{R}^{n \times d_{\text{in}}} \rightarrow \mathbb{R}^{n^k \times d_{\text{out}}}$  over compact domains  $K \subset \mathbb{R}^{n \times d_{\text{in}}}$ .

**Theorem 1.** *The model  $\mathbf{F}^k$  is set-to- $k$ -edge universal.*

A corollary of Theorem 1 establishes a general set-to-hypergraph universal models:

**Theorem 2.** *The model  $(\mathbf{F}^1, \dots, \mathbf{F}^k)$  is set-to-hypergraph universal.*

Our main tool for proving Theorem 1 is a characterization of the equivariant set-to- $k$ -edge *polynomials*  $\mathbf{P}^k$ . This characterization can be seen as a generalization of the characterization of set-to-set equivariant polynomial recently appeared in (Segol & Lipman, 2020).

We consider an arbitrary set-to- $k$ -edge continuous mapping  $\mathbf{G}^k(\mathbf{X})$  over a compact set  $K \subset \mathbb{R}^{n \times d_{\text{in}}}$ . Since  $\mathbf{G}^k$  is equivariant we can assume  $K$  is symmetric, i.e.,  $\sigma \cdot K = K$  for all  $\sigma \in S_n$ . The proof consists of three parts: (i) Characterization of the equivariant set-to- $k$ -edge polynomials  $\mathbf{P}^k$ . (ii) Showing that every equivariant continuous set-to- $k$ -edge function  $\mathbf{G}^k$  can be approximated by some  $\mathbf{P}^k$ . (iii) Every  $\mathbf{P}^k$  can be approximated by our model  $\mathbf{F}^k$ .

Before providing the full proof which contains some technical derivations let us provide a simpler universality proof (under some mild conditions) for the set-to-2-edge model,  $\mathbf{F}^2$ , based on the Singular Value Decomposition (SVD).

##### 4.1. A simple proof for universality of $\mathbf{F}^2$

It is enough to consider the  $d_{\text{out}} = 1$  case; the general case is implied by applying the argument for each output feature dimension independently. Let  $\mathbf{G}^2$  be an arbitrary continuous equivariant set-to-2-edge function  $\mathbf{G}^2 : K \subset \mathbb{R}^{n \times d_{\text{in}}} \rightarrow \mathbb{R}^{n \times n}$ . We want to approximate  $\mathbf{G}^2$  with our model  $\mathbf{F}^2$ . First, note that without losing generality we can assume

$\mathbf{G}^2(\mathbf{X})$  has a simple spectrum (i.e., eigenvalues are all different) for all  $\mathbf{X} \in K$ . Indeed, if this is not the case we can always choose  $\lambda > 0$  sufficiently large and consider  $\mathbf{G}^2 + \lambda \text{diag}(1, 2, \dots, n)$ . This diagonal addition does not change the 2-edge values assigned by  $\mathbf{G}^2$ , and it guarantee simple spectrum using standard hermitian matrix eigenvalue perturbation theory (see e.g., (Stewart, 1990), Section IV:4).

Now let  $\mathbf{G}^2(\mathbf{X}) = \mathbf{U}(\mathbf{X})\mathbf{\Sigma}(\mathbf{X})\mathbf{V}(\mathbf{X})^T$  be the SVD of  $\mathbf{G}^2(\mathbf{X})$ , where  $\mathbf{U} = [\mathbf{u}_1, \dots, \mathbf{u}_n]$  and  $\mathbf{V} = [\mathbf{v}_1, \dots, \mathbf{v}_n]$ . Since  $\mathbf{G}^2(\mathbf{X})$  has a simple spectrum,  $\mathbf{U}, \mathbf{V}, \mathbf{\Sigma}$  are all continuous in  $\mathbf{X}$ ;  $\mathbf{\Sigma}$  is unique, and  $\mathbf{U}, \mathbf{V}$  are unique up to a sign flip of the singular vectors (i.e., columns of  $\mathbf{U}, \mathbf{V}$ ) (O’Neil, 2005). Let us first assume that the singular vectors can be chosen uniquely also up to a sign, later we show how we achieve this with some additional mild assumption.

Now, uniqueness of the SVD together with the equivariance of  $\mathbf{G}^2$  imply that  $\mathbf{U}, \mathbf{V}$  are continuous *set-to-set* equivariant and  $\mathbf{\Sigma}$  is continuous *set invariant* function:

$$\begin{aligned} & (\sigma \cdot \mathbf{U}(\mathbf{X}))\mathbf{\Sigma}(\mathbf{X})(\sigma \cdot \mathbf{V}(\mathbf{X}))^T \\ &= \sigma \cdot \mathbf{G}(\mathbf{X}) = \mathbf{G}(\sigma \cdot \mathbf{X}) \\ &= \mathbf{U}(\sigma \cdot \mathbf{X})\mathbf{\Sigma}(\sigma \cdot \mathbf{X})\mathbf{V}(\sigma \cdot \mathbf{X})^T. \end{aligned}$$

Lastly, since  $\phi$  is set-to-set universal there is a choice of its parameters so that it approximates arbitrarily well the equivariant set-to-set function  $\mathbf{Y} = [\mathbf{U}, \mathbf{V}, \mathbf{1}\mathbf{1}^T\mathbf{\Sigma}]$ . The  $\psi$  component can be chosen by noting that  $\mathbf{G}^2(\mathbf{X})_{i_1, i_2} = \sum_{j=1}^n \sigma_j \mathbf{U}_{i_1, j} \mathbf{V}_{i_2, j} = \mathbf{p}(\beta(\mathbf{Y})_{i_1, i_2, :})$ , where  $\sigma_j$  are the singular values, and  $\mathbf{p} : \mathbb{R}^{6n} \rightarrow \mathbb{R}$  is a cubic polynomial. To conclude pick  $\mathbf{m}$  to approximate  $\mathbf{p}$  sufficiently well so that  $\psi \circ \beta \circ \phi$  approximates  $\mathbf{G}^2$  to the desired accuracy.

To achieve uniqueness of the singular vectors up-to a sign we can add, e.g., the following assumption:  $\mathbf{1}^T \mathbf{u}_i(\mathbf{X}) \neq 0 \neq \mathbf{1}^T \mathbf{v}_i(\mathbf{X})$  for all singular vectors and  $\mathbf{X} \in K$ . Using this assumption we can always pick  $\mathbf{u}_i(\mathbf{X}), \mathbf{v}_i(\mathbf{X})$  in the SVD so that  $\mathbf{1}^T \mathbf{u}_i(\mathbf{X}) > 0, \mathbf{1}^T \mathbf{v}_i(\mathbf{X}) > 0$ , for all  $i \in [n]$ .

We now move to the general proof.

##### 4.2. Equivariant set-to- $k$ -edge polynomials

We start with a characterization of the set-to- $k$ -edge equivariant polynomials  $\mathbf{P}^k : \mathbb{R}^{n \times d_{\text{in}}} \rightarrow \mathbb{R}^{n^k \times d_{\text{out}}}$ .

We need some more notation. Given a vector  $\mathbf{x} \in \mathbb{R}^d$ , and a multi-index  $\alpha \in [n]^d$ , we set  $\mathbf{x}^\alpha = \prod_{i=1}^d x_i^{\alpha_i}$ ;  $|\alpha| = \sum_{i=1}^d \alpha_i$ ; and define accordingly  $\mathbf{X}^\alpha = (\mathbf{x}_1^\alpha, \dots, \mathbf{x}_n^\alpha)^T$ . Given two tensors  $\mathbf{A} \in \mathbb{R}^{n^{k_1}}, \mathbf{B} \in \mathbb{R}^{n^{k_2}}$  we use the notation  $\mathbf{A} \otimes \mathbf{B} \in \mathbb{R}^{n^{k_1+k_2}}$  to denote the tensor-product, defined by  $(\mathbf{A} \otimes \mathbf{B})_{i_1, i_2} = \mathbf{A}_{i_1} \mathbf{B}_{i_2}$ , where  $i_1, i_2$  are suitable multi-indices. Lastly, we denote by  $\alpha = (\alpha^1, \dots, \alpha^k)$  a vector of multi-indices  $\alpha^i \in [n]^d$ , and  $\mathbf{X}^\alpha = \mathbf{X}^{\alpha^1} \otimes \dots \otimes \mathbf{X}^{\alpha^k}$ .

**Theorem 3.** An equivariant set-to- $k$ -edge polynomial  $\mathbf{P}^k : \mathbb{R}^{n \times d_{in}} \rightarrow \mathbb{R}^{n^k \times d_{out}}$  can be written as

$$\mathbf{P}^k(\mathbf{X}) = \sum_{\alpha} \mathbf{X}^{\alpha} \otimes \mathbf{q}_{\alpha}(\mathbf{X}) \quad (5)$$

where  $\alpha = (\alpha^1, \dots, \alpha^k)$ ,  $\alpha^i \in [n]^{d_{in}}$ , and  $\mathbf{q}_{\alpha} : \mathbb{R}^{n \times d_{in}} \rightarrow \mathbb{R}^{d_{out}}$  are  $S_n$  invariant polynomials.

As an example, consider the graph case, where  $k = 2$ . Equivariant set-to-2-edge polynomials take the form:

$$\mathbf{P}^k(\mathbf{X}) = \sum_{\alpha^1, \alpha^2} \mathbf{X}^{\alpha^1} \otimes \mathbf{X}^{\alpha^2} \otimes \mathbf{q}_{\alpha^1, \alpha^2}(\mathbf{X}), \quad (6)$$

and coordinate-wise

$$\mathbf{P}_{ijl}^k(\mathbf{X}) = \sum_{\alpha^1, \alpha^2} \mathbf{x}_i^{\alpha^1} \mathbf{x}_j^{\alpha^2} q_{\alpha^1, \alpha^2, l}(\mathbf{X}). \quad (7)$$

The general proof idea is to consider an arbitrary equivariant set-to- $k$ -edge polynomial  $\mathbf{P}^k$  and use its equivariance property to show that it has the form as in equation 5. This is done by looking at a particular output entry  $\mathbf{P}_{i^0}^k$ , where say  $i^0 = (1, 2, \dots, k)$ . Then the proof considers two subsets of permutations: First, the subgroup of all permutations  $\sigma \in S_n$  that fixes the numbers  $1, 2, \dots, k$ , i.e.,  $\sigma(i^0) = i^0$ , but permute everything else freely; this subgroup is denoted  $\text{stab}(i^0)$ . Second, permutations of the form  $\sigma = (1 \ i_1)(2 \ i_2) \cdots (k \ i_k)$ , where  $\mathbf{i} \in [n]^k$ . Each of these permutation subsets reveals a different part in the structure of the equivariant polynomial  $\mathbf{P}^k$  and its relation to invariant polynomials.

As before, it is enough to prove Theorem 3 for  $d_{out} = 1$ . Let  $i^0 = (1, 2, \dots, k)$  and consider any permutation  $\sigma \in \text{stab}(i^0)$ . Then from equivariance of  $\mathbf{P}^k$  we have

$$\mathbf{P}_{i^0}^k(\mathbf{X}) = \mathbf{P}_{\sigma^{-1}(i^0)}^k(\mathbf{X}) = \mathbf{P}_{i^0}^k(\sigma \cdot \mathbf{X}),$$

and  $\sigma \cdot \mathbf{X} = (\mathbf{x}_1, \dots, \mathbf{x}_k, \mathbf{x}_{\sigma^{-1}(k+1)}, \dots, \mathbf{x}_{\sigma^{-1}(n)})^T$ . That is  $\mathbf{P}_{i^0}^k$  is invariant to permuting its last  $n - k$  elements  $\mathbf{x}_{k+1}, \dots, \mathbf{x}_n$ ; we say that  $\mathbf{P}_{i^0}^k$  is  $S_{n-k}$  invariant. We next prove that  $S_{n-k}$  invariance can be written using a combination of  $S_n$  invariant polynomials and tensor products of  $\mathbf{x}_1, \dots, \mathbf{x}_k$ :

**Lemma 1.** Let  $p(\mathbf{X}) = p(\mathbf{x}_1, \dots, \mathbf{x}_k, \mathbf{x}_{k+1}, \dots, \mathbf{x}_n)$  be  $S_{n-k}$  invariant polynomial. That is invariant to permuting the last  $n - k$  terms. Then

$$p(\mathbf{X}) = \sum_{\alpha} \mathbf{x}_1^{\alpha^1} \cdots \mathbf{x}_k^{\alpha^k} q_{\alpha}(\mathbf{X}), \quad (8)$$

where  $q_{\alpha}$  are  $S_n$  invariant polynomials.

We prove this lemma in the supplementary material. So now we know that  $\mathbf{P}_{i^0}^k$  has the form equation 8. On the other

hand let  $\mathbf{i}$  be an arbitrary multi-index and consider the permutation  $\sigma = (1 \ i_1)(2 \ i_2) \cdots (k \ i_k)$ . Again by permutation equivariance of  $\mathbf{P}^k$  we have

$$\begin{aligned} \mathbf{P}_{i_1 i_2 \cdots i_k}^k(\mathbf{X}) &= \mathbf{P}_{\sigma^{-1}(i_0)}^k(\mathbf{X}) = \mathbf{P}_{i_0}^k(\sigma \cdot \mathbf{X}) \\ &= \sum_{\alpha} \mathbf{x}_{i_1}^{\alpha^1} \cdots \mathbf{x}_{i_k}^{\alpha^k} q_{\alpha}(\mathbf{X}), \end{aligned}$$

which is a coordinate-wise form of equation 5 with  $d_{out} = 1$ .

**Approximating  $\mathbf{G}^k$  with a polynomial  $\mathbf{P}^k$ .** We denote for an arbitrary tensor  $\mathbf{A} \in \mathbb{R}^{a \times b \times \cdots \times c}$  its infinity norm by  $\|\mathbf{A}\|_{\infty} = \max_{\mathbf{i}} |\mathbf{A}_{\mathbf{i}}|$ .

**Lemma 2.** Let  $\mathbf{G}^k : K \subset \mathbb{R}^{n \times d_{in}} \rightarrow \mathbb{R}^{n^k \times d_{out}}$  be a continuous equivariant function over a symmetric domain  $K \subset \mathbb{R}^{n \times d_{out}}$ . For an arbitrary  $\epsilon > 0$ , there exists an equivariant polynomial  $\mathbf{P}^k : \mathbb{R}^{n \times d_{in}} \rightarrow \mathbb{R}^{n^k \times d_{out}}$  so that

$$\max_{\mathbf{X} \in K} \left\| \mathbf{G}^k(\mathbf{X}) - \mathbf{P}^k(\mathbf{X}) \right\|_{\infty} < \epsilon.$$

This is a standard lemma, similar to (Yarotsky, 2018; Maron et al., 2019c; Segol & Lipman, 2020); for completeness we provide a proof in the supplementary.

**Approximating  $\mathbf{P}^k$  with a network  $\mathbf{F}^k$ .** The final component of the proof of Theorem 1 is showing that an equivariant polynomial  $\mathbf{P}^k$  can be approximated over  $K$  using a network of the form in equation 2. The key is to use the characterization of Theorem 3 and write  $\mathbf{P}^k$  in a similar form to our model in equation 2:

$$\mathbf{P}_{i,:}^k(\mathbf{X}) = p(\beta(\mathbf{H}(\mathbf{X}))_{i,:}), \quad (9)$$

where  $\mathbf{H} : K \rightarrow \mathbb{R}^{n \times d_1}$  defined by  $\mathbf{H}(\mathbf{X})_{i,:} = [\mathbf{x}_i, \mathbf{q}(\mathbf{X})]$ , where  $\mathbf{q}(\mathbf{X}) = [\mathbf{q}_{\alpha_1}(\mathbf{X}), \dots, \mathbf{q}_{\alpha_m}(\mathbf{X})]$ , and  $\alpha_1, \alpha_2, \dots, \alpha_m$  are all the multi-indices participating in the sum in equation 5. Note that

$$\beta(\mathbf{H}(\mathbf{X}))_{i,:} = [\mathbf{x}_{i_1}, \mathbf{q}(\mathbf{X}), \mathbf{x}_{i_2}, \mathbf{q}(\mathbf{X}), \dots, \mathbf{x}_{i_k}, \mathbf{q}(\mathbf{X})].$$

Therefore,  $\mathbf{p} : \mathbb{R}^{d_2} \rightarrow \mathbb{R}^{d_{out}}$  is chosen as the polynomial

$$\mathbf{p} : [\mathbf{x}_1, \mathbf{y}, \mathbf{x}_2, \mathbf{y}, \dots, \mathbf{x}_k, \mathbf{y}] \mapsto \sum_{\alpha} \mathbf{x}_1^{\alpha^1} \cdots \mathbf{x}_k^{\alpha^k} \mathbf{y}_{\alpha},$$

where  $\mathbf{y} = [\mathbf{y}_{\alpha_1}, \dots, \mathbf{y}_{\alpha_m}] \in \mathbb{R}^{m d_{out}}$ , and  $\mathbf{y}_{\alpha_i} \in \mathbb{R}^{d_{out}}$ .

In view of equation 9 all we have left is to choose  $\phi$  and  $\psi$  (i.e.,  $\mathbf{m}$ ) to approximate  $\mathbf{H}$ ,  $\mathbf{p}$  (resp.) to a desired accuracy. We detail the rest of the proof in the supplementary.

**Universality of the set-to-hypergraph model.** Theorem 2 follows from Theorem 1 by considering a set-to-hypergraph continuous function  $\mathbf{G}$  as a collection  $\mathbf{G}^k$  of set-to- $k$ -edge functions and approximating each one using our

model  $\mathbf{F}^k$ . Note that universality still holds if  $\mathbf{F}^1, \dots, \mathbf{F}^K$  all share the  $\phi$  part of the network (assuming sufficient width  $d_1$ ).

Note that a set-to- $k$ -edge model (in equation 2) is not universal when approximating set-to-hypergraph functions:

**Proposition 1.** *The set-to-2-edge model,  $\mathbf{F}^2$ , cannot approximate general set-to-graph functions.*

The proof is in the supplementary; it shows that even the constant function that outputs 1 for 1-edges (nodes), and 0 for 2-edges cannot be approximated by a set-to-2-edge model  $\mathbf{F}^2$ .

**Relation to similarity learning** Previous models suggested for learning pairwise relations in sets were mostly of the form  $\mathbf{H}^2(\mathbf{X}) = \mathbf{m}(\phi(\mathbf{x}_i), \phi(\mathbf{x}_j))$  (Hsu et al., 2017; Bromley et al., 1994; Simo-Serra et al., 2015; Zagoruyko & Komodakis, 2015; Bell & Bala, 2015; Ahmed et al., 2015; Vo & Hays, 2016). This model is similar to the model suggested in this paper for the  $k = 2$  case but is not universal for two main reasons: (i) The same MLP is used both for 1-edge (nodes or self-loops) predictions and 2-edge prediction; Proposition 1 implies that the model is not universal in this case; (ii) The model used in the role of  $\phi$  is a element-wise MLP which is not set-to-set universal (Segol & Lipman, 2020).

**Relation to hypergraph equivariant networks.** Our model’s constituents  $\phi, \beta, \psi$  are all built from certain equivariant linear layers and entry-wise non-linearity. Therefore, our model is an instance of the general equivariant hypergraph networks framework (Maron et al., 2019b). The benefit in our suggested model compared to the general equivariant model is that it is much more efficient in terms computational complexity and memory footprint. In particular, it uses only one basis function for the  $\psi$  (scaled identity, without counting features) in contrast to  $\text{bell}(2k)$  in the full equivariant model, and can be used without constructing  $k$ -order tensors explicitly in memory. Even though the model is lean in terms of number of parameters (i.e., uses less basis functions) it is proven it to be universal (i.e., with maximal expressive power). As far as we are aware, this fact was not known before, even for the full equivariant models when approximating set-to-hypergraph functions and restricting the tensor order in the network.

## 5. Applications

We have tested our model on a collection of learning tasks that fall into the categories: (1) Set-to-2-edge tasks; (2) Set-to-graph tasks; and (3) Set-to-3-edge tasks.

**Variants of our model.** We used  $\mathbf{F}^2$ ,  $(\mathbf{F}^1, \mathbf{F}^2)$ , and  $\mathbf{F}^3$  (resp.) for these learning tasks.  $\phi$  is implemented using

DeepSets (Zaheer et al., 2017) with 5 layers with output dimension  $d_1 \in \{5, 10, 80, 512\}$ ;  $\psi$  is implemented with an MLP,  $\mathbf{m}$ , with  $\{2, 3, 6\}$  layers with input dimension  $d_2$  defined by  $d_1$  and  $\beta$ .  $\beta$  is implemented according to equation 3: for  $k = 2$  it uses  $d_2 = 2 * d_1$  output features and for  $k = 3$ ,  $d_2 = 3 * d_1$  output features. We name this model S2G. For the  $k = 2$  case we have also tested a more general (but not more expressive) broadcasting  $\beta$  defined using the full equivariant basis  $\mathbb{R}^n \rightarrow \mathbb{R}^{n^2}$  from (Maron et al., 2019b) that contains  $\text{bell}(3) = 5$  basis operations: (1-2) as in  $\beta$ ; (3) broadcast the nodes values to the diagonal; map the sum of all nodes to the (4) diagonal; and (5) to all of the entries. This broadcasting layer gives  $d_2 = 5 * d_1$ ; we name this model S2G+.

More architecture, implementation and hyper-parameter details can be found in the supplementary.

**Baselines.** We compare our results to the following baselines: (1) a model as in equation 2 but with a non-universal set-to-set function as  $\phi$ , namely, an MLP on each element (vector) in the set; we use the same loss as is used in our model; we name this model MLP. For the particle physics application we also used: (2) The same architecture as (1) but with a triplet loss (Weinberger et al., 2006) on the learned representations based on  $l_2$  distance; we name this baseline (TRI). (3) A non-learnable geometric-based baseline described later.

### 5.1. Set-to-2-edges

The first type of problems we tackle involve learning set-to-2-edge functions. Here, each training example is a pair  $(\mathbf{X}, \mathbf{Y})$  where  $\mathbf{X}$  is a set  $\mathbf{X} = (\mathbf{x}_1, \mathbf{x}_2, \dots, \mathbf{x}_n)^T \in \mathbb{R}^{n \times d_{in}}$  and  $\mathbf{Y} \in \{0, 1\}^{n \times n}$  is an adjacency matrix (the diagonal of  $\mathbf{Y}$  is ignored).

#### 5.1.1. PARTITIONING FOR PARTICLE PHYSICS

In particle physics experiments, such as the Large Hadron Collider (LHC), beams of incoming particles are collided at high energies. The results of the collision are outgoing particles, whose properties (such as the trajectory) are measured by detectors surrounding the collision point.

A critical low-level task for analyzing this data is to associate the particle trajectories to their progenitor, which can be formalized as partitioning sets of particle trajectories into subsets according to their unobserved point of origin in space. This task is referred to as vertex reconstruction in particle physics and is illustrated in Figure 3a.

The measured particle trajectories correspond to elements in the input set and nodes in the output graph, and the parameters that characterize them serve as the node features. An edge between two nodes indicates that the two particles

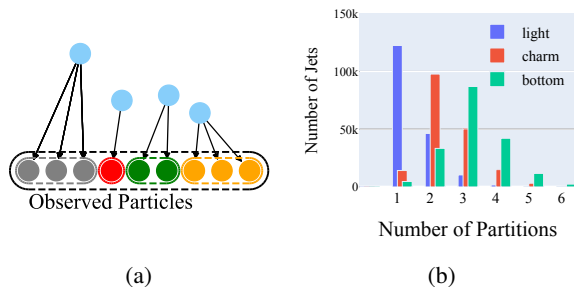


Figure 3. (a) Illustration of a particle physics experiment. The observed particles originate from different points in space called vertices (light blue dots). The task is to partition the set of observed particles based on their point of origin. (b) Distribution of the number of partitions in each type of set.

come from a common progenitor or vertex. We enforce that the adjacency matrix of the graph encodes a valid partitioning of tracks to vertices.

Vertex reconstruction propagates to a number of downstream data analysis tasks, such as particle identification (a classification problem). Therefore, improvements to the vertex reconstruction has significant impact on the sensitivity of collider experiments. We consider multiple quantities to quantify the performance of the partitioning: the F1 score, the Rand Index (RI), and the Adjusted Rand Index ( $ARI = (RI - \mathbb{E}[RI]) / (1 - \mathbb{E}[RI])$ ). We will consider three different types (or *flavors*) of particle sets (called *jets*) corresponding to three different fundamental data generating processes labeled bottom-jets, charm-jets, and light-jets (B/C/L). The important distinction between the flavors is the typical number of partitions in each set. Figure 3b shows the distribution of the number of partitions (vertices) in each flavor: bottom jets typically have multiple partitions; charm jets also have multiple partitions, but fewer than bottom jets; and light jets typically have only one partition.

**Dataset.** Algorithms for particle physics are typically designed with high-fidelity simulators, which can provide labeled training data. These algorithms are then applied to and calibrated with real data collected by the LHC experiments. Our simulated samples are created with a standard simulation package called PYTHIA (Sjstrand et al., 2015) and the detector is simulated with DELPHES (de Favereau et al., 2014). We use this software to generate synthetic datasets for the three flavors of jets. The generated sets are small, ranging from 2 to 14 elements each.

**Results** We compare the results of our model (S2G and S2G+) trained to minimize the F1 score to a typical baseline algorithm used in particle physics - the Adaptive Vertex Reconstruction (AVR) algorithm (Waltenberger, 2011). We ran each model (except AVR) 11 times, and evaluated the

Model	F1	RI	ARI
AVR	0.565	0.612	0.318
B MLP	0.606±0.001	0.672±0.004	0.409±0.004
B TRI	0.595±0.002	0.665±0.004	0.387±0.004
B S2G	0.646±0.003	0.736±0.004	0.491±0.006
B S2G+	<b>0.655±0.004</b>	<b>0.747±0.006</b>	<b>0.508±0.007</b>
C AVR	0.695	0.650	0.326
C MLP	0.729±0.001	0.694±0.002	0.405±0.004
C TRI	0.718±0.001	0.706±0.003	0.414±0.004
C S2G	0.747±0.001	0.727±0.003	0.457±0.004
C S2G+	<b>0.751±0.002</b>	<b>0.733±0.003</b>	<b>0.467±0.005</b>
L AVR	0.970	0.965	0.922
L MLP	<b>0.973±0.001</b>	<b>0.970±0.001</b>	0.926±0.003
L TRI	0.904±0.002	0.888±0.002	0.758±0.006
L S2G	0.972±0.001	<b>0.970±0.001</b>	<b>0.931±0.003</b>
L S2G+	0.971±0.002	0.969±0.002	0.929±0.003

Table 1. Performance of partitioning for three types of jets.

model F1 score, RI and ARI over the test set for each run. The results are shown in Table 1. For bottom and charm jets, which have secondary vertices, all of our models reach comparable results and improve over the AVR baseline by about 10% in all performance metrics. In light-jets, without secondary decays, our models reach similar F1 scores.

### 5.1.2. LEARNING DELAUNAY TRIANGULATIONS

In a second set-to-2-edge task we test our model’s ability to learn Delaunay triangulations, namely given a set of planar points we want to predict the Delaunay edges between pairs of points, see e.g., (De Berg et al., 1997) Chapter 9. We generated 50k planar point sets as training data and 5k planar point sets as test data; the point sets,  $X \in \mathbb{R}^{n \times 2}$ , were uniformly sampled in the unit square, and a ground truth matrix in  $\{0, 1\}^{n \times n}$  was computed per point set using a Delaunay triangulation algorithm. The number of points in a set,  $n$ , is either 50 or varies and is randomly chosen from  $\{20, \dots, 80\}$ . Training was stopped after 100 epochs. See more implementation details in the supplementary material. In Table 2 we report accuracy of prediction as well as precision recall and F1 score. Evidently, both S2G and S2G+ achieve comparable results while outperforming the baseline MLP. See also Figure 4 for visualizations of several triangulations predicted with the trained model versus ground truth.

	Accuracy	Precision	Recall	F1
$n = 50$				
S2G	0.984	0.927	0.926	0.926
S2G+	0.983	0.927	0.925	0.926
MLP	0.939	0.769	0.647	0.702
$n \in \{20, \dots, 80\}$				
S2G	0.947	0.736	0.934	0.799
S2G+	0.947	0.735	0.934	0.798
MLP	0.917	0.658	0.772	0.686

Table 2. Results on the Delaunay triangulation task.

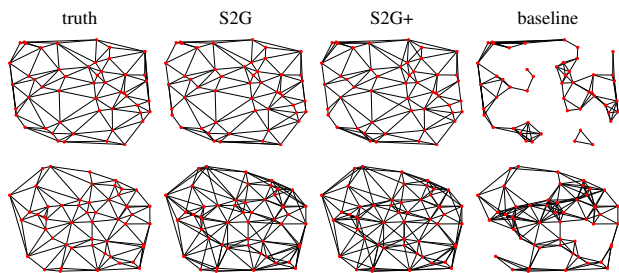


Figure 4. Results of Delaunay triangulation learning. Top:  $n = 50$ ; Bottom:  $n \in \{20, \dots, 80\}$ .

dataset	PPGN	PPGN+S2G	MPNN	MPNN+S2G
BBBP	67.19±1.72	66.50±1.88	64.60±2.23	65.45±1.89
BACE	76.10±0.60	77.31±1.62	77.48±2.60	76.40±3.25
TOXCAST	62.04±0.47	61.98±0.68	<b>56.95±3.06</b>	<b>63.28±0.78</b>
HIV	75.09±2.71	74.30±3.18	<b>69.38±1.94</b>	<b>72.63±2.48</b>
TOX21	72.88±0.93	72.90±0.93	<b>67.33±0.83</b>	<b>73.22±0.79</b>
SIDER	56.05±1.87	57.47±1.72	<b>56.08±1.23</b>	<b>61.74±1.27</b>
CLINTOX	75.75±8.36	77.93±5.78	<b>58.98±7.45</b>	<b>76.18±3.42</b>

Table 3. MoleculeNet Graph classification with and without set-to-graph input data augmentation. Significant improvements when using S2G are marked in bold, while other results show differences that are within the statistical error.

## 5.2. Set-to-Graphs

One of the main learning tasks in graph analysis is graph classification. Our goal here is to try and improve existing graph learning models, and in particular Graph Neural Networks (GNNs). Since existing GNNs are not graph-to-graph universal we suggest the following procedure to potentially improve their performance: First, compute new node and edge features from the initial set of node features using  $\mathbf{F}^1$  and  $\mathbf{F}^2$  (resp.), and then concatenate these to the original input and feed this augmented input to the GNN.

For the set-to-graph model, we use  $\phi$ ,  $\beta$  as described above, and 2 different MLPs as  $\psi$ : one for the nodes (for  $\mathbf{F}^1$ ), and one for the edges (for  $\mathbf{F}^2$ ). For the GNN we have used two GNN variants: a message-passing neural network (Gilmer et al., 2017) (MMPN), and Provably Powerful Graph Networks (PPGN) (Maron et al., 2019a); implementation details can be found in the supplementary materials. We compared performance after training the same GNN in two ways: with the original input data, and with the S2G-augmented input data. We used graph datasets from (Wu et al., 2018) using the Open Graph Benchmark (OGB, 2019). All tasks considered are binary or multi-binary graph classification.

Results are presented in table 3. We report mean  $\pm$  standard deviation of the AUC-ROC of the models on the test sets. Note that in several datasets (bold in table) there is a significant performance boost when S2G augments MPNN; while for other datasets and for the PPGN model (that is more expressive than MPNN yet heavier computationally and memory-wise) there is no noticeable improvement.

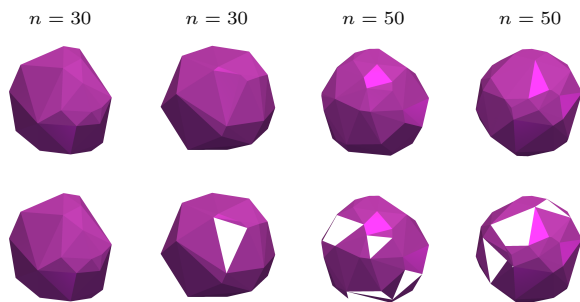


Figure 5. Convex hull learning. Top: ground truth. Bottom: predicted.

## 5.3. Set to 3-edges

In the last experiment, we demonstrate learning of set-to-3-edge function. The learning task we target is finding supporting triangles in the convex hull of a set of points in  $\mathbb{R}^3$ . In this scenario, the input is a point set  $\mathbf{X} \in \mathbb{R}^{n \times 3}$ , and the function we wanted to learn is  $\mathbf{F}^3 : \mathbb{R}^{n \times 3} \rightarrow \mathbb{R}^{n^3}$  where the output is a probability for each triplet of nodes (triangle)  $\{\mathbf{x}_{i_1}, \mathbf{x}_{i_2}, \mathbf{x}_{i_3}\}$  to belong to the triangular mesh that describes the convex hull of  $\mathbf{X}$ .

Note that storing 3-rd order tensors in memory is not feasible, hence we concentrate on a *local* version of the problem: Given a point set  $\mathbf{X} \subset \mathbb{R}^3$ , identify the triangles within the  $K$ -Nearest-Neighbors of each point that belong to the convex hull of the entire point set  $\mathbf{X}$ . We used  $K = 10$ . Therefore, for broadcasting ( $\beta$ ) from point data to 3-edge data, instead of holding a 3-rd order tensor in memory we broadcast only the subset of  $K$ -NN neighborhoods. This allows working with high-order information with relatively low memory footprint. Furthermore, since we want to consider 3-edges (triangles) with no order we used invariant universal set model (DeepSets again) as  $m$ .

We tested our models on two types of data: Gaussian and spherical. For both types we draw point sets in  $\mathbb{R}^3$  i.i.d. from standard normal distribution,  $\mathcal{N}(0, 1)$ , where for the spherical data we normalize each point to unit length. We generated  $20k$  point set samples as a training set,  $2k$  for validation and another  $2k$  for test set. Point sets are in  $\mathbb{R}^{n \times 3}$ , where  $n = 30$ ,  $n = 50$ , and  $n \in [20, 100]$ . As a baseline, we used MLP. The F1 scores and AUC-ROC of the predicted convex hull triangles are shown in Table 4, where our models out-perform the baseline. See Figure 5 for several examples of triangles predicted using our trained model compared to the ground truth.

	# points	F1	AUC-ROC
Spherical			
S2G	30	0.780	0.988
MLP	30	0.425	0.885
S2G	50	0.686	0.975
MLP	50	0.424	0.890
S2G	20-100	0.535	0.953
MLP	20-100	0.354	0.885
Gaussian			
S2G	30	0.707	0.996
MLP	30	0.275	0.946
S2G	50	0.661	0.997
MLP	50	0.254	0.974
S2G	20-100	0.552	0.994
MLP	20-100	0.187	0.969

Table 4. Convex hull learning.

See Figure 5 for several examples of triangles predicted using our trained model compared to the ground truth.



## Acknowledgments

HS, NS and YL were supported in part by the European Research Council (ERC Consolidator Grant, "LiftMatch" 771136), the Israel Science Foundation (Grant No. 1830/17) and by a research grant from the Carolito Stiftung (WAIC). JS and EG were supported by the NSF-BSF Grant 2017600 and the ISF Grant 2871/19. KC was supported by the National Science Foundation under the awards ACI-1450310, OAC-1836650, and OAC-1841471 and by the Moore-Sloan data science environment at NYU.

## References

- Open graph benchmark. <https://ogb.stanford.edu/>, 2019.
- Ahmed, E., Jones, M., and Marks, T. K. An improved deep learning architecture for person re-identification. In *Proceedings of the IEEE conference on computer vision and pattern recognition*, pp. 3908–3916, 2015.
- Aljalbout, E., Golkov, V., Siddiqui, Y., Strobel, M., and Cremers, D. Clustering with deep learning: Taxonomy and new methods. *arXiv preprint arXiv:1801.07648*, 2018.
- Bell, S. and Bala, K. Learning visual similarity for product design with convolutional neural networks. *ACM Transactions on Graphics (TOG)*, 34(4):98, 2015.
- Bromley, J., Guyon, I., LeCun, Y., Säckinger, E., and Shah, R. Signature verification using a "siamese" time delay neural network. In *Advances in neural information processing systems*, pp. 737–744, 1994.
- Chen, Z., Villar, S., Chen, L., and Bruna, J. On the equivalence between graph isomorphism testing and function approximation with gnns. *arXiv preprint arXiv:1905.12560*, 2019.
- Chopra, S., Hadsell, R., LeCun, Y., et al. Learning a similarity metric discriminatively, with application to face verification. In *CVPR (1)*, pp. 539–546, 2005.
- Cohen, T. and Welling, M. Group equivariant convolutional networks. In *International conference on machine learning*, pp. 2990–2999, 2016a.
- Cohen, T. S. and Welling, M. Steerable CNNs. (1990):1–14, 2016b. URL <http://arxiv.org/abs/1612.08498>.
- Cohen, T. S., Geiger, M., Köhler, J., and Welling, M. Spherical cnns. *arXiv preprint arXiv:1801.10130*, 2018.
- De Berg, M., Van Kreveld, M., Overmars, M., and Schwarzkopf, O. Computational geometry. In *Computational geometry*, pp. 1–17. Springer, 1997.
- de Favereau, J., Delaere, C., Demin, P., Giammanco, A., Lematre, V., Mertens, A., and Selvaggi, M. Delphes 3: a modular framework for fast simulation of a generic collider experiment. *Journal of High Energy Physics*, 2014(2), Feb 2014. ISSN 1029-8479. doi: 10.1007/jhep02(2014)057. URL [http://dx.doi.org/10.1007/JHEP02\(2014\)057](http://dx.doi.org/10.1007/JHEP02(2014)057).
- Dieleman, S., De Fauw, J., and Kavukcuoglu, K. Exploiting cyclic symmetry in convolutional neural networks. *arXiv preprint arXiv:1602.02660*, 2016.
- Esteves, C., Allen-Blanchette, C., Makadia, A., and Daniilidis, K. 3d object classification and retrieval with spherical cnns. *arXiv preprint arXiv:1711.06721*, 2017.
- Gilmer, J., Schoenholz, S. S., Riley, P. F., Vinyals, O., and Dahl, G. E. Neural message passing for quantum chemistry. In *International Conference on Machine Learning*, pp. 1263–1272, 2017.
- Hsu, Y.-C., Lv, Z., and Kira, Z. Learning to cluster in order to transfer across domains and tasks. *arXiv preprint arXiv:1711.10125*, 2017.
- Ilse, M., Tomczak, J. M., and Welling, M. Attention-based deep multiple instance learning. *arXiv preprint arXiv:1802.04712*, 2018.
- Jiang, Y. and Verma, N. Meta-learning to cluster. *arXiv preprint arXiv:1910.14134*, 2019.
- Keriven, N. and Peyré, G. Universal invariant and equivariant graph neural networks. *CoRR*, abs/1905.04943, 2019. URL <http://arxiv.org/abs/1905.04943>.
- Kingma, D. P. and Ba, J. Adam: A method for stochastic optimization. *arXiv preprint arXiv:1412.6980*, 2014.
- Kipf, T. N. and Welling, M. Semi-supervised classification with graph convolutional networks. *arXiv preprint arXiv:1609.02907*, 2016.
- Kondor, R., Son, H. T., Pan, H., Anderson, B., and Trivedi, S. Covariant compositional networks for learning graphs. *arXiv preprint arXiv:1801.02144*, 2018.
- Krizhevsky, A., Sutskever, I., and Hinton, G. E. Imagenet classification with deep convolutional neural networks. In *Advances in neural information processing systems*, pp. 1097–1105, 2012.
- LeCun, Y., Bottou, L., Bengio, Y., Haffner, P., et al. Gradient-based learning applied to document recognition. *Proceedings of the IEEE*, 86(11):2278–2324, 1998.
- Maron, H., Ben-Hamu, H., Serviansky, H., and Lipman, Y. Provably powerful graph networks. *arXiv preprint arXiv:1905.11136*, 2019a.

- Maron, H., Ben-Hamu, H., Shamir, N., and Lipman, Y. Invariant and equivariant graph networks. In *International Conference on Learning Representations*, 2019b. URL <https://openreview.net/forum?id=Syx72jC9tm>.
- Maron, H., Fetaya, E., Segol, N., and Lipman, Y. On the universality of invariant networks. *arXiv preprint arXiv:1901.09342*, 2019c.
- Morris, C., Ritzert, M., Fey, M., Hamilton, W. L., Lenssen, J. E., Rattan, G., and Grohe, M. Weisfeiler and leman go neural: Higher-order graph neural networks. *arXiv preprint arXiv:1810.02244*, 2018.
- O’Neil, K. A. Critical points of the singular value decomposition. *SIAM journal on matrix analysis and applications*, 27(2):459–473, 2005.
- Qi, C. R., Su, H., Mo, K., and Guibas, L. J. Pointnet: Deep learning on point sets for 3d classification and segmentation. *Proc. Computer Vision and Pattern Recognition (CVPR), IEEE*, 1(2):4, 2017.
- Ravanbakhsh, S., Schneider, J., and Poczos, B. Equivariance through parameter-sharing. *arXiv preprint arXiv:1702.08389*, 2017.
- Rydh, D. A minimal set of generators for the ring of multisymmetric functions. In *Annales de l’institut Fourier*, volume 57, pp. 1741–1769, 2007.
- Sannai, A., Takai, Y., and Cordonnier, M. Universal approximations of permutation invariant/equivariant functions by deep neural networks. *arXiv preprint arXiv:1903.01939*, 2019.
- Segol, N. and Lipman, Y. On universal equivariant set networks. In *International Conference on Learning Representations*, 2020. URL <https://openreview.net/forum?id=HkxTwrKDB>.
- Simo-Serra, E., Trulls, E., Ferraz, L., Kokkinos, I., Fua, P., and Moreno-Noguer, F. Discriminative learning of deep convolutional feature point descriptors. In *Proceedings of the IEEE International Conference on Computer Vision*, pp. 118–126, 2015.
- Sjstrand, T., Ask, S., Christiansen, J. R., Corke, R., Desai, N., Ilten, P., Mrenna, S., Prestel, S., Rasmussen, C. O., and Skands, P. Z. An introduction to pythia 8.2. *Computer Physics Communications*, 191:159177, Jun 2015. ISSN 0010-4655. doi: 10.1016/j.cpc.2015.01.024. URL <http://dx.doi.org/10.1016/j.cpc.2015.01.024>.
- Stewart, G. W. Matrix perturbation theory. 1990.
- Vaswani, A., Shazeer, N., Parmar, N., Uszkoreit, J., Jones, L., Gomez, A. N., Kaiser, L., and Polosukhin, I. Attention is all you need, 2017.
- Veličković, P., Cucurull, G., Casanova, A., Romero, A., Liò, P., and Bengio, Y. Graph Attention Networks. pp. 1–12, 2017. URL <http://arxiv.org/abs/1710.10903>.
- Vo, N. N. and Hays, J. Localizing and orienting street views using overhead imagery. In *European conference on computer vision*, pp. 494–509. Springer, 2016.
- Waltenberger, W. RAVE: A detector-independent toolkit to reconstruct vertices. *IEEE Trans. Nucl. Sci.*, 58:434–444, 2011. doi: 10.1109/TNS.2011.2119492.
- Weiler, M., Geiger, M., Welling, M., Boomsma, W., and Cohen, T. 3D Steerable CNNs: Learning Rotationally Equivariant Features in Volumetric Data. 2018. URL <http://arxiv.org/abs/1807.02547>.
- Weinberger, K. Q., Blitzer, J., and Saul, L. K. Distance metric learning for large margin nearest neighbor classification. In *Advances in neural information processing systems*, pp. 1473–1480, 2006.
- Worrall, D. and Brostow, G. Cubenet: Equivariance to 3d rotation and translation. In *Proceedings of the European Conference on Computer Vision (ECCV)*, pp. 567–584, 2018.
- Worrall, D. E., Garbin, S. J., Turmukhambetov, D., and Brostow, G. J. Harmonic networks: Deep translation and rotation equivariance. In *Proceedings of the IEEE Conference on Computer Vision and Pattern Recognition*, pp. 5028–5037, 2017.
- Wu, Z., Ramsundar, B., Feinberg, E. N., Gomes, J., Geniesse, C., Pappu, A. S., Leswing, K., and Pande, V. Moleculenet: a benchmark for molecular machine learning. *Chemical science*, 9(2):513–530, 2018.
- Xu, K., Hu, W., Leskovec, J., and Jegelka, S. How powerful are graph neural networks? In *International Conference on Learning Representations*, 2019. URL <https://openreview.net/forum?id=ryGs6iA5Km>.
- Yarotsky, D. Universal approximations of invariant maps by neural networks. *arXiv preprint arXiv:1804.10306*, 2018.
- Zagoruyko, S. and Komodakis, N. Learning to compare image patches via convolutional neural networks. In *Proceedings of the IEEE conference on computer vision and pattern recognition*, pp. 4353–4361, 2015.
- Zaheer, M., Kottur, S., Ravanbakhsh, S., Poczos, B., Salakhutdinov, R. R., and Smola, A. J. Deep sets. In *Advances in neural information processing systems*, pp. 3391–3401, 2017.

---

## Set2Graph: Learning Graphs From Sets: Supplementary Material

---

### 6. Architectures and hyper-paramteres

All of our models follow the formula  $\mathbf{F}^k = \psi \circ \beta \circ \phi$ , where  $\phi$  is a set-to-set model,  $\beta$  is a *non-learnable* broadcasting set-to-graph layer, and  $\psi$  is a simple graph-to-graph network using only a single Multi-Layer Perceptron (MLP) acting on each  $k$ -edge feature vector independently. We note that all the hyper-parameters were chosen using the validation scores only.

**Notation.** "DeepSets / MLP of widths [256, 256, 5]" means that we use a DeepSets/MLP network with 3 layers, and each layer's output feature size is its corresponding argument in the array (e.g. the first and second layers have output feature size of 256, while the third layer output feature size is 5). Between the layers we use ReLU as a non linearity.

**Partitioning for particle physics applications.** In our models  $\phi$  is implemented using DeepSets (Zaheer et al., 2017) with 5 layers of width [256, 256, 256, 256, 5].  $\beta$  is broadcasting the node features in one of the following ways: for model S2G it creates 2 features for each input feature, and S2G+ creates 5 features for each input feature (2 features out of the 5 vanish outside the diagonal).  $\psi$  is implemented with 2 edge-wise MLP of widths [256, 1], ending as the edge probability. As a loss, we used a combination of soft F1 score loss and an edge-wise binary cross-entropy loss.

Instead of using a max or sum pooling in DeepSets layers, we used a self-attention mechanism based on (Ilse et al., 2018) and (Vaswani et al., 2017):

$$\text{Attention}(\mathbf{X}) = \text{softmax}\left(\frac{\tanh f_1(\mathbf{X}) \cdot f_2(\mathbf{X})^T}{\sqrt{d_{\text{small}}}}\right) \cdot \mathbf{X} \quad (10)$$

Where  $f_1, f_2$  are implemented by two single MLPs of width  $d_{\text{small}} = d_{\text{in}}/10$ .

We used a grid search for the following hyper-parameters: learning rate in the range of  $\{1e-5, 3e-5, 1e-4, 3e-4, 1e-3, 3e-3\}$ , DeepSets layers width of  $\{64, 128, 256, 512\}$ , number of layers of  $\{3, 4, 5\}$ ,  $\psi$  (MLP) of widths  $\{128, 256, 512, [128, 256, 128]\}$ , and with or without attention mechanism in DeepSets. We chose to use 250 epochs with early stopping based on validation score, batch size of 2048, adam optimizer (Kingma & Ba, 2014). Our

models train in less than 2 hours on a single Tesla V100 GPU.

The deep learning baselines are implemented as follows: **MLP** is implemented similarly to S2G, with the exception that instead of using DeepSets as  $\phi$ , we use MLP of widths [512, 512, 512, 512, 5]. **TRI** uses a siamese MLP of widths [256, 256, 256, 256, 5] to extract node features, and the edge logits are the l2 distances between the nodes. For loss, we use triplets loss (Weinberger et al., 2006) - we draw random triplets *anchor, neg, pos* where *anchor* and *pos* are of the same cluster, and *neg* is of a different cluster, and the loss is defined as <sup>1</sup>

$$L_i = \min(d_{l2}(\text{anch}_i, \text{pos}_i) - d_{l2}(\text{anch}_i, \text{neg}_i) + 2, 0)$$

The dataset is made of training, validation and test set with 543544, 181181 and 181182 instances accordingly. Each of the sets contains all three flavors: bottom, charm and light jets roughly in the same amount, while the flavor of each instance is not part of the input.

Each model is being evaluated 11 times for stability in the same manner: (1) training over the dataset, stopping when the F1 score over the validation set is minimal. (2) Predicting the clusters of the test set. (3) Separate the 3 flavors and calculating the metrics for each flavor. Eventually, we have 11 scores for each combination of metrics, flavor and model, and we report the mean $\pm$ std. Note that the AVR is evaluated only once since it is not a learning algorithm.

**Learning Delaunay triangulation.** In our models  $\phi$  is implemented using with 7 layers of width [500, 500, 500, 1000, 500, 500, 80].  $\beta$  is broadcasting as before for models S2G and S2G+, thus ending with 160 or 400 features per edge.  $\psi$  is implemented with 2 edge-wise MLP of widths [1000, 1000, 1], ending as the edge probability. We use edge-wise binary cross-entropy loss. The implementation of **MLP** baseline is identical except for  $\phi$  which is an MLP with the same amount of layers and widths.

We searched learning rate from  $\{1e-2, 1e-3, 1e-4\}$ .

**Set to graph.** Our models include set2graph followed by a GNN, trained together (as a single network). In our models  $\phi$  is implemented using DeepSets with 5 layers of width [256, 256, 256, 256, 10].  $\beta$  is of S2G, thus ending with 20

---

<sup>1</sup>A natural disadvantage of the triplets loss is that it cannot learn from sets with a single cluster, or sets with size 2.

dataset	size	# of tasks	average # of node	median # of nodes	# of runs
BBBP	2039	1	24.1	23	100
BACE	1513	1	34.1	33	100
TOXCAST	8576	617	18.8	16	50
HIV	41127	1	25.5	23	10
TOX21	7831	12	18.5	16	50
SIDER	1427	27	33.6	25	100
CLINTOX	1477	2	26.1	23	100

Table 5. MoleculeNet graph classification information.

features.  $\psi$  uses 2 different MLPs for the edges and nodes (i.e., diagonal and off-diagonal)<sup>2</sup>, each MLP is of widths [256, 1], ending as the probability. The GNN that followed are either PPGN with 3 layers, or MPNN with 3 layers with shared weights. As a loss, we use a binary cross-entropy loss on the targets.

We used a grid search as following: For all models, learning rate from  $\{1e-5, 3e-5, 1e-4, 3e-4, 1e-3, 3e-3\}$ . For PPGN we also searched each layer’s width from  $\{16, 32, 64\}$ . For the S2G models, the number of new learned features was searched from  $\{\text{\#original-node-features}, 64, 128\}$ , and with or without attention mechanism in the DeepSets model (equation 6). We used early stopping based on the validation score. In order to get more stable results, we ran each model 10/50/100 times (exact numbers in Table 5) and present the mean $\pm$ std AUC-ROC based on those multiple runs.

**Set to 3-edges.** In our models  $\phi$  is implemented using DeepSets of width [512, 512, 512]. In this task, the models predict over a subset of all possible supporting triangles of the convex hull, also referred to as faces, so we do not maintain 3-rd order tensors in the memory. We aggregate all the faces which lie within the KNN ( $k = 10$ ) of one of the nodes. In order to be invariant to the order of the 3 nodes in a face, each triplets is viewed as a set and fed to a DeepSets of widths [64, 64, 64], max-pooled, and then to an MLP of widths [256, 128, 1]. As a loss, we used a combination of soft F1 score loss and an face-wise binary cross-entropy loss. The baseline is identical except that  $\phi$  is implemented by MLP of widths [1024, 1024, 512], and the second DeepSets is replaced by an MLP of widths [128, 128, 64].

For hyper-parameters search, we examined learning rates from  $\{1e-5, 3e-5, 1e-4, 3e-4, 1e-3, 3e-3\}$ , and DeepSets models of width  $\{64, 128, 256, 512\}$ .

<sup>2</sup>The use of 2 different MLPs for the diagonal and off-diagonal is necessary to separate between the learning of  $\mathbf{F}^1$ , the set-to-set function, and  $\mathbf{F}^2$ , the set-to-2-edges function.

## 7. Proofs

*Proof (of Lemma 1).* First we expand  $p$  as

$$p(\mathbf{X}) = \sum_{\alpha} \mathbf{x}_1^{\alpha_1} \cdots \mathbf{x}_k^{\alpha_k} p_{\alpha}(\mathbf{x}_{k+1}, \dots, \mathbf{x}_n), \quad (11)$$

where  $p_{\alpha}$  are  $S_{n-k}$  invariant polynomials. Since  $S_{n-k}$  invariant polynomials with variables  $\mathbf{x}_{k+1}, \dots, \mathbf{x}_n$  are generated by the power-sum multi-symmetric polynomials

$$\sum_{i=k+1}^n \mathbf{x}_i^{\alpha} = \sum_{i=1}^n \mathbf{x}_i^{\alpha} - \sum_{i=1}^k \mathbf{x}_i^{\alpha},$$

with  $|\alpha| \leq n - k$ , see e.g., (Rydh, 2007), we have that each  $p_{\alpha}(\mathbf{x}_{k+1}, \dots, \mathbf{x}_n) = \sum_{\alpha} \mathbf{x}_1^{\alpha_1} \cdots \mathbf{x}_k^{\alpha_k} r_{\alpha}(\mathbf{X})$ , for some  $S_n$  invariant polynomials  $r_{\alpha}$ . Plugging this in equation 11 proves the lemma.  $\square$

*Proof (Lemma 2).* We can assume  $d_{\text{out}} = 1$ . The general case is proved by finding approximating polynomial to each output feature coordinate. Let  $\epsilon > 0$ . Using Stone-Weierstrass we can find a polynomial  $\mathbf{Q} : K \rightarrow \mathbb{R}^{n^k}$  so that  $\max_{\mathbf{X} \in K} \|\mathbf{G}^k(\mathbf{X}) - \mathbf{Q}(\mathbf{X})\|_{\infty} < \epsilon$ . Let

$$\mathbf{P}^k(\mathbf{X}) = \frac{1}{n!} \sum_{\sigma \in S_n} \sigma \cdot \mathbf{Q}(\sigma^{-1} \cdot \mathbf{X}).$$

Then  $\mathbf{P}^k$  is equivariant and since  $\mathbf{G}^k$  is also equivariant we have

$$\begin{aligned} & \|\mathbf{G}^k(\mathbf{X}) - \mathbf{P}^k(\mathbf{X})\|_{\infty} \\ &= \frac{1}{n!} \left\| \sum_{\sigma \in S_n} \sigma \cdot \left( \mathbf{G}^k(\sigma^{-1} \cdot \mathbf{X}) - \mathbf{Q}(\sigma^{-1} \cdot \mathbf{X}) \right) \right\|_{\infty} \\ &< \frac{1}{n!} \sum_{\sigma \in S_n} \epsilon = \epsilon. \end{aligned}$$

$\square$

**Approximating  $\mathbf{P}^k$  with a network  $\mathbf{F}^k$ .** We set a target  $\epsilon > 0$ . Let  $U \supset H(K)$  be a compact  $\epsilon$ -neighborhood of  $H(K)$ .  $p$  is uniformly continuous over  $\cup_i \beta(U)_{i,:}$ . Choose  $m$  so to be an  $\epsilon/2$ -approximation to  $p$  over  $\cup_i \beta(U)_{i,:}$ . Let  $\delta$  be so that for  $\mathbf{Y}, \mathbf{Y}' \in U$ ,  $\|\mathbf{Y} - \mathbf{Y}'\|_{\infty} < \delta$  implies  $\|p(\beta(\mathbf{Y})) - p(\beta(\mathbf{Y}'))\|_{\infty} < \epsilon/2$ . Now choose  $\phi$  so that it is  $\delta_0$ -approximation to  $H$  over  $K$  where  $\delta_0 < \min\{\delta, \epsilon\}$ . This can be done since  $\phi$  is a universal set-to-set model as in (Segol & Lipman, 2020). Lastly, putting all the pieces together we get for all  $i$ :

$$\begin{aligned} & |p(\beta(H(\mathbf{X}))_{i,:}) - m(\beta(\phi(\mathbf{X}))_{i,:})| \leq \\ & |p(\beta(H(\mathbf{X}))_{i,:}) - p(\beta(\phi(\mathbf{X}))_{i,:})| + \\ & |p(\beta(\phi(\mathbf{X}))_{i,:}) - m(\beta(\phi(\mathbf{X}))_{i,:})| < \epsilon. \end{aligned}$$

*Proof (Proposition 1).* Consider the case  $k = 2$  and the constant function set-to-graph function  $\mathbf{G}(\mathbf{X}) = \mathbf{I}$ , where  $\mathbf{I}$  is the identity  $n \times n$  matrix; that is  $\mathbf{G}$  learns the constant value 1 for 1-edges (nodes), and 0 for 2-edges. Since  $\phi$  is equivariant we have that  $\phi(\mathbf{1}) = \mathbf{1} \otimes \mathbf{a} = \mathbf{1}\mathbf{a}^T$ , for some vector  $\mathbf{a} \in \mathbb{R}^{d_1}$ . Therefore  $\beta(\phi(\mathbf{1}))_{i_1, i_2, :} = [\mathbf{a}, \mathbf{a}]$  and  $\mathbf{m}(\beta(\phi(\mathbf{1}))) = \mathbf{m}([\mathbf{a}, \mathbf{a}]) = b \in \mathbb{R}$ . We get that  $\mathbf{F}^2(\mathbf{1})_{i_1, i_2, :} = b$  and  $\|\mathbf{I} - \mathbf{F}^2(\mathbf{1})\|_\infty \geq 1/2$ .  $\square$

## 8. Physics background.

The Large Hadron Collider (LHC) is the world's highest energy particle collider, located at the CERN laboratory in Geneva, and is used to study the fundamental particles of nature and their interactions. The LHC collides proton beams at high energy, and these collisions produce many new particles, which may be unstable or lead to subsequent particle production. For instance, the production of quarks (fundamental particles that make up protons, neutrons, and other hadrons) will lead to the production of many hadrons and eventually be manifest as a spray of particles called a *jet*. The collisions take place in a vacuum, but the collision point is surrounded by large detectors that measure the outgoing particles that are stable enough to reach the detector several centimeters away. In order to probe the properties of particles that are unstable, we need to infer which “flavor” of quark was the progenitor particle that led to a jet. This classification is performed in many stages, and we focus on a particular aspect of it known as vertex reconstruction, which we describe below.

The location of the initial proton-proton collision is referred to as the primary vertex. Several particles emanating from the primary vertex are stable, will reach the detector, and will be part of the observed jet. Other particles will be unstable and travel a few millimeters before decaying in what is referred to as a secondary vertex. The unstable particles are not observed; however, the trajectories of the stable charged particles will be measured by detectors located around the collision point. Due to the presence of magnetic fields in the detector, the trajectories of the charged particles are helical. The helical trajectories are called *tracks*, and are summarized by 6 numbers, called the perigee parameters, along with a covariance matrix quantifying the uncertainty of their measurement.

Vertex reconstruction can be composed into two parts, vertex finding and vertex fitting. Vertex finding refers to partitioning the tracks into vertices, and vertex fitting is computing the most likely origin point in space for a collection of tracks. In the standard vertex reconstruction algorithms, these two parts are often intertwined and done together. In this application we perform the partitioning without performing the actual geometrical fit. From the physics point of view, once we improve the partitioning, the identification of the jets flavor is naturally improved.